Training and temperature effects of epitaxial and polycrystalline $Ni_{80}Fe_{20}/Fe_{50}Mn_{50}$ exchange biased bilayers

Marian Fecioru-Morariu,[1] Jerzy Wrona,[2] Cristian Papusoi,[3] and Gernot Güntherodt[1]
[1]*Physikalisches Institut (IIA), RWTH Aachen University, 52056 Aachen, Germany*
[2]*Department of Electronics, AGH University of Science and Technology, 30-059 Krakow, Poland*
[3]*SPINTEC, CEA/CNRS, 38054 Grenoble Cedex 9, France*
(Received 11 June 2007; revised manuscript received 5 October 2007; published 28 February 2008)

For exchange biased bilayers of $Ni_{80}Fe_{20}/Fe_{50}Mn_{50}$, the effects of crystalline structure on the training effect of the exchange bias field (H_{EB}) and of the coercive field (H_C) have been investigated for (001)- and (110)-oriented epitaxial as well as polycrystalline thin film samples. The training effect of H_{EB} and H_C at 5 K is strongest for the polycrystalline sample as compared to the (110)-oriented sample. The training effect is found to originate from the hysteresis cycle-number dependence of H_1, the switching field of the descending branch of the hysteresis loop. A very good qualitative agreement is observed between the cycle-number dependence of H_{EB} and of the fraction of pinned uncompensated moments of an antiferromagnet (AFM) monolayer. In the temperature range between 5 and 300 K, H_{EB} and H_C are found to depend strongly on the crystalline structure as well as orientation of the ferromagnet (FM)/AFM bilayers.

DOI: 10.1103/PhysRevB.77.054441 PACS number(s): 75.70.−i, 75.30.Et, 75.50.Ee, 75.60.−d

I. INTRODUCTION

The exchange coupling at the interface between a ferromagnet (FM) and an antiferromagnet (AFM), discovered in 1956 by Meiklejohn and Bean,[1] causes a unidirectional anisotropy in the FM layer. As a consequence, the hysteresis loop of the FM layer is shifted along the magnetic field axis and simultaneously an enhanced coercivity in addition to that of the isolated FM layer is observed.[2–4] The shift of the FM/AFM hysteresis loop is called exchange bias field, H_{EB}.

The use of the exchange bias (EB) effect for pinning the magnetization of an FM layer in spin valves led to intense research activities in this field.[2–4] The complexity of the EB effect and the various unknown structural and magnetic properties at the FM/AFM interface gave rise to rather contradictory results which made it difficult to find a generally accepted interpretation of the EB phenomena. However, various models were proposed in order to understand the microscopic origin of EB.[5–8] For instance, the domain state (DS) model[8,9] for EB, initially proposed for the EB of a high-anisotropy Ising-type AFM such as CoO, has been recently found to explain also the EB properties of metallic AFMs with low and intermediate anisotropies, such as FeMn (Ref. 10) and IrMn.[11]

The AFM γ-$Fe_{50}Mn_{50}$ is one of the most studied AFMs in EB systems. Recently, first principles electronic structure calculations[12,13] have shown that the fcc γ-FeMn has a noncollinear ($3Q$) spin structure. Experimental studies of epitaxial $Ni_{80}Fe_{20}/Fe_{50}Mn_{50}$ bilayers revealed that there is no correlation between the strength of biasing and the compensated or uncompensated nature of the FM/AFM interfaces with different crystallographic orientations.[14,15] The training effect which describes the variation of H_{EB} with the number of hysteresis loop cycles has also been intensively studied recently. Various experimental and theoretical studies of the training effect have been performed with respect to the AFM anisotropy and "spin flop" effects,[16] the formation of perpendicular domain walls in the AFM,[17] the dynamics of the hysteresis loops,[18] and the role of interfacial domain walls.[19] However, for understanding the EB and its training effect a comparison between epitaxial and polycrystalline FM/AFM bilayers is of utmost importance and has not been performed yet for any EB system.

In this paper we report on a comparative study of the influence of different crystalline structures and crystallographic orientations on training effect and temperature dependence of EB in $Ni_{80}Fe_{20}/Fe_{50}Mn_{50}$ bilayers. The samples have been grown epitaxially in (001) and (110) orientations, and also in polycrystalline form. The training effect and the temperature dependence of the exchange bias field H_{EB} and of the coercive field H_C are found to depend strongly on the crystalline structure and crystallographic orientation of the bilayers. For all samples, the training effect of H_{EB} is closely connected with the decrease of the fraction of pinned uncompensated moments of an AFM monolayer upon field cycling. The experimental results are interpreted in the framework of the DS model.

II. SAMPLE DEPOSITION AND CHARACTERIZATION

Cu single crystal substrates with the (001) and (110) orientations were used in order to induce epitaxial growth of $Ni_{80}Fe_{20}$ and $Fe_{50}Mn_{50}$ layers. Since no high-quality epitaxial growth can be obtained for $Ni_{80}Fe_{20}/Fe_{50}Mn_{50}$ on (111)-oriented Cu single crystals,[14] we have not used such substrate crystals. However, for comparison we used a Si/SiO_2 substrate with a 50 nm thick Cu seed layer for the deposition of the polycrystalline $Ni_{80}Fe_{20}/Fe_{50}Mn_{50}$ sample. Prior to the deposition the Cu single crystal substrates were cleaned in an ultrahigh vacuum chamber using successive Ar sputtering cycles followed by annealing at temperatures up to 850 °C. The chemical cleanliness of the Cu single crystal substrate surfaces was examined *in situ* using x-ray photoelectron spectroscopy (XPS). The surface crystalline orientation was checked *in situ* by low energy electron diffraction (LEED). Figure 1 shows the XPS spectra and LEED patterns (left-

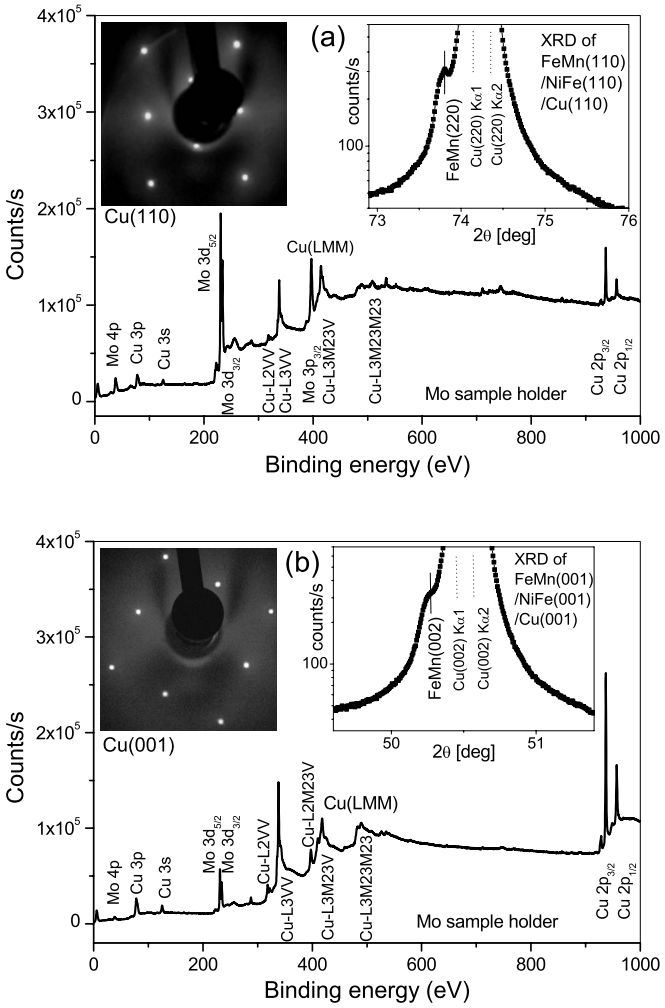

FIG. 1. XPS spectrum and LEED pattern (left-hand side insets) of the Cu single crystal substrates with the orientations: (a) (110) and (b) (001). The right-hand side insets show part of the XRD scans of $Ni_{80}Fe_{20}/Fe_{50}Mn_{50}$ grown on the respective Cu single crystal substrates.

hand side insets) of the Cu single crystal substrates with (a) (110) and (b) (001) orientations. The XPS spectra show clean surfaces of the Cu single crystal substrates without contaminations by other chemical elements. The Mo peaks in the XPS spectra are due to the substrate holder. The LEED patterns show that the two different (110) and (001) substrate orientations were well obtained.

Samples with the layer sequence [substrate: Cu(001) or Cu(110) or $Si/SiO_2/Cu(50\ nm)$]/$Ni_{80}Fe_{20}(10\ nm)/Fe_{50}Mn_{50}(10\ nm)/Au(5\ nm)$ were deposited in a molecular beam epitaxy system with a base pressure of 10^{-10} mbar. All depositions were carried out at room temperature using e-beam evaporation of Fe, Ni, Mn, and Au. A Knudsen cell was used for Cu evaporation. The deposition rates for both binary alloys were 0.04 nm/s and they were kept constant during deposition to within 1%. In order to initialize the exchange bias at room temperature (for γ-$Fe_{50}Mn_{50}$, $T_{Néel}$ = 220 °C), all samples were deposited in the presence of an in-plane magnetic field $H_{deposition}$=250 Oe. Hence, $H_{deposition}$ has been applied along the [100] and [$\bar{1}$10] direction during the deposition of the (001)- and (110)-oriented samples, respectively.

In situ LEED measurements were also performed after deposition of the $Ni_{80}Fe_{20}$ and $Fe_{50}Mn_{50}$ layers, in order to check their epitaxial quality. We observed that the $Ni_{80}Fe_{20}$ layer had grown epitaxially on both Cu single crystal substrates with (001) and (110) orientations. $Fe_{50}Mn_{50}$ was grown on top of the $Ni_{80}Fe_{20}$ layer. We still observed similar LEED patterns after deposition of $Fe_{50}Mn_{50}$ on top of $Cu(110)/Ni_{80}Fe_{20}(110)$, indicating a good epitaxial growth of the $Fe_{50}Mn_{50}$ layer. For the (001) orientation, no LEED pattern was observed after deposition of the $Fe_{50}Mn_{50}$ layer on top of $Cu(001)/Ni_{80}Fe_{20}(001)$. This may indicate the appearance of some structural defects during the deposition of the (001)-oriented $Fe_{50}Mn_{50}$ which reduce the quality of the epitaxial growth for the (001) orientation. These results are also supported by *ex situ* $\theta-2\theta$ x-ray diffraction (XRD) scans of the FM/AFM bilayers (right-hand side insets of Fig. 1). Only the peaks corresponding to the two different orientations {001} and {110} of $Fe_{50}Mn_{50}$ were observed. Furthermore, the intensity of the (220) $Fe_{50}Mn_{50}$ peak was higher in comparison with that of the (002) $Fe_{50}Mn_{50}$ peak (see right-hand side insets of Fig. 1), confirming again a higher-quality epitaxial growth of the (110)-oriented $Fe_{50}Mn_{50}$ as compared to that of the (001)-orientated $Fe_{50}Mn_{50}$.

The third sample, grown on a $Si/SiO_2/Cu(50\ nm)$ substrate, was prepared under the same conditions as the epitaxial samples. The results of the XRD θ-2θ scans of the polycrystalline sample reveal the preferred (111) orientation of the Cu/NiFe/FeMn trilayer. However, weak (100) and (311) reflections were also observed. Since Cu, NiFe, and γ-FeMn all have fcc crystalline structures with almost identical lattice parameters, their diffraction peaks cannot be easily distinguished. Moreover, we showed elsewhere[10] by scanning tunneling microscopy that this sample has a structure containing small crystalline grains with mean diameter of 18 nm.

Magnetic measurements were performed using a superconducting quantum interference device (SQUID) magnetometer. The samples were cooled from room temperature to 5 K in an applied field of H_{cool}=1 T parallel to $H_{deposition}$. During the measurements the magnetic field was applied in the plane of the samples along the direction of $H_{deposition}$ and H_{cool}. Subsequently, the temperature was gradually increased up to room temperature through a sequence of intermediate temperatures. At each of these temperatures, the applied field was cycled from $+H_{cool}$ to $-H_{cool}$ and back to $+H_{cool}$ in order to measure a hysteresis cycle. Prior to the measurements, at 5 K, the magnetic field was cycled 12 times and the hysteresis loops were measured in order to study the training effect. The switching fields of the two branches of the hysteresis loops, H_1 for the descending and H_2 for the ascending branch, were used to estimate H_{EB} and the coercive field H_C according to $H_{EB}=(H_1+H_2)/2$ and $H_C=|H_1-H_2|/2$, respectively.

III. RESULTS AND DISCUSSION

Figure 2(a) shows the magnetic training effect of H_{EB} of the samples containing epitaxial (110) $Fe_{50}Mn_{50}$ and (001)

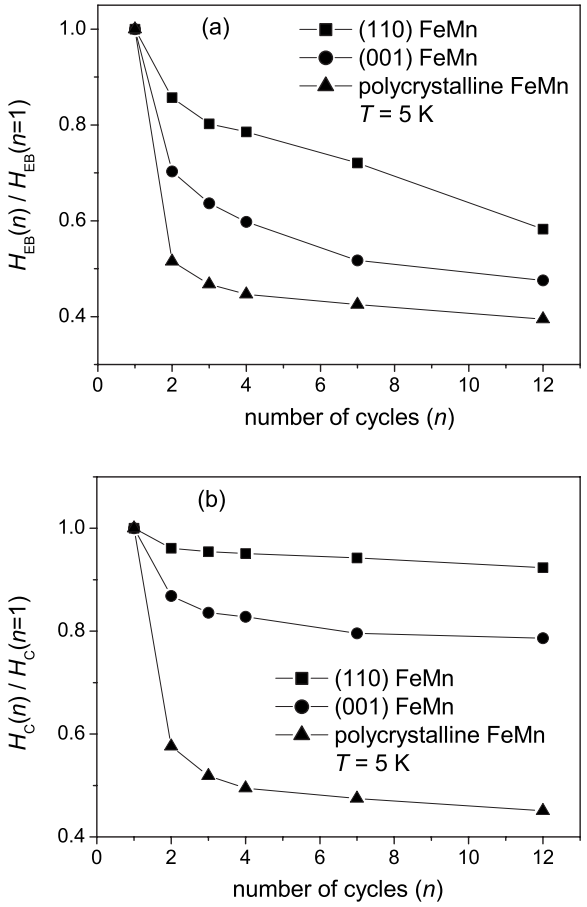

FIG. 2. Training effect in terms of the number (n) of hysteresis cycles at $T=5$ K with respect to that of $n=1$ of (a) H_{EB} and (b) H_C of $Ni_{80}Fe_{20}/Fe_{50}Mn_{50}$ exchange biased bilayers containing (110)- and (001)- oriented $Fe_{50}Mn_{50}$, and polycrystalline $Fe_{50}Mn_{50}$ layers.

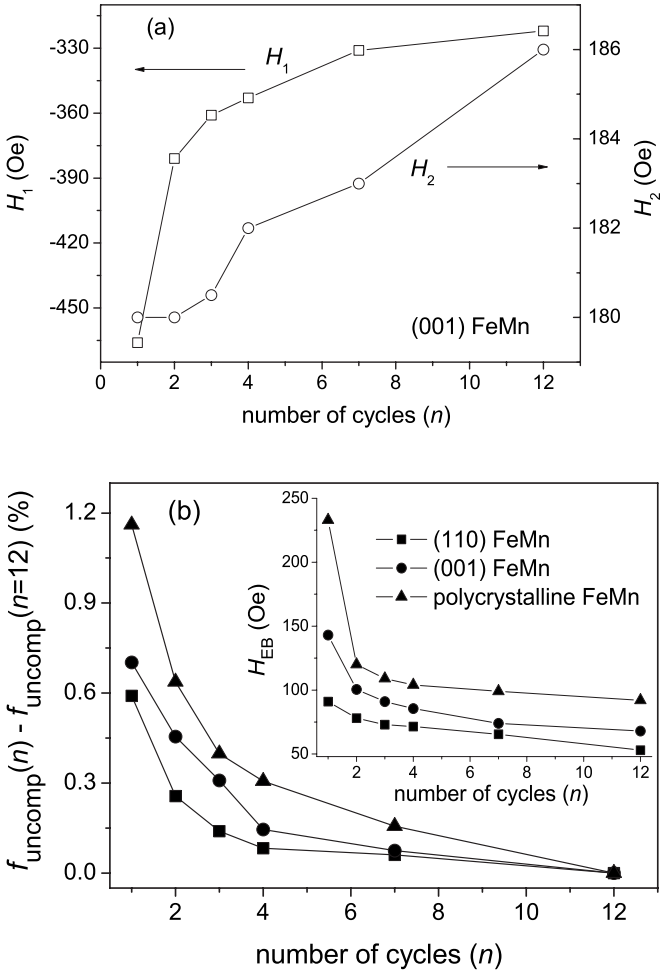

FIG. 3. (a) Field cycling number (n) dependence at $T=5$ K of the switching fields H_1 and H_2 of the descending and ascending branches, respectively, of the hysteresis loops of the (001)- oriented $Ni_{80}Fe_{20}/Fe_{50}Mn_{50}$ bilayers. (b) Decrease of the fraction of pinned uncompensated moments of an AFM monolayer $f_{uncomp}(n)$-$f_{uncomp}(n=12)$ at $T=5$ K as function of field cycle number (n) for different orientations of $Fe_{50}Mn_{50}$ in $Ni_{80}Fe_{20}/Fe_{50}Mn_{50}$ bilayers. The inset shows for comparison the training effect of the non-normalized H_{EB}.

$Fe_{50}Mn_{50}$ as well as polycrystalline $Fe_{50}Mn_{50}$, measured at 5 K after field cooling. One can see that for all samples the most significant decrease of H_{EB} takes place between the first and second hysteresis cycles, the effect being weaker for further hysteresis loops. The training effect is found to depend strongly on the crystalline structure of $Fe_{50}Mn_{50}$. We show for the epitaxial (110) $Fe_{50}Mn_{50}$ that H_{EB} measured after cycling the magnetic field 12 times is 40% smaller than its value for the first hysteresis loop, after field cooling to 5 K. Under the same conditions the corresponding decrease in H_{EB} for (001) $Fe_{50}Mn_{50}$ is found to be more than 50%. The most significant training effect, however, is observed in the case of the polycrystalline $Fe_{50}Mn_{50}$ sample. For this sample H_{EB} extracted from the second hysteresis loop has decreased by 50% from that of the first hysteresis loop. After cycling the magnetic field up to 12 times, the decrease of H_{EB} of the polycrystalline sample is found to be about 60% of the value of the first loop.

The coercive field H_C of all the above three samples shows qualitatively a similar training effect as observed for H_{EB}. In Fig. 2(b), for the (110)-oriented sample the decrease of H_C due to the training effect after 12 field cycles is only about 10% compared to that after the first hysteresis loop. H_C of the (001)-oriented sample decreases by about 20% after 12 field cycles. However, analogously to H_{EB}, H_C of the polycrystalline sample shows the most significant decrease by 45% after 12 field cycles.

We have also observed that the training effect originates from the cycle-number (n) dependence of H_1, as shown, for example, in Fig. 3(a) for the (001)-oriented sample. H_2 shows a different dependence on n, as compared to that of H_1. The quantitative n dependence of H_1 is much stronger than that of H_2 [see Fig. 3(a)]. Consequently, the training effect of H_{EB} and H_C is determined by the cycle-number (n) dependence of H_1, while the influence of H_2 is much smaller. The different strengths of n dependencies of H_1 and H_2, which were also observed by Hochstrat *et al.* for NiO/Fe bilayers,[20] indicate that the two branches belonging to H_1 and H_2 follow different mechanisms of magnetization reversal. A similar behavior was observed for CoO/Co bilayers where coherent rotation has been observed at H_2, while do-

main nucleation and wall propagation have been assigned in the vicinity of H_1.[21]

The DS model[8,10] for EB considers the presence of defects[22] throughout the finite AFM lattice, leading to the formation of AFM domains. Consequently, an irreversible DS magnetization develops in the AFM during the field cooling. In contact with an FM layer, the irreversible DS magnetization gives rise to the EB effect.[8,10] Within this model the training effect is attributed to the rearrangement of the AFM domain structure, which results in a partial loss of the irreversible DS magnetization of the AFM layer during field cycling.[8,9,23] This has been observed as a vertical shift of the hysteresis loop of, e.g., Co/CoO bilayers.[8,9,23] This loss of net magnetization leads to a reduction of H_{EB}. Monte Carlo simulations of a single-crystalline, Ising-type AFM lattice with nonmagnetic defects support qualitatively the above observations of the training effect.[8] We have shown in Fig. 2 that the training effect of H_{EB} and H_C depends on the quality of the epitaxial growth of the $Fe_{50}Mn_{50}$ layer. On the other hand, our LEED and XRD studies of (110)- and (001)-oriented $Fe_{50}Mn_{50}$ clearly indicate a higher-quality epitaxial growth of the (110) orientation with less structural defects as compared to that of the (001) orientation. Hence, the rearrangement of the AFM domain structure during field cycling, which arises from the presence of defects in the AFM lattice, is more pronounced and effective in (001) $Fe_{50}Mn_{50}$ than in (110) $Fe_{50}Mn_{50}$. This explains why the training effect is stronger for the (001) $Fe_{50}Mn_{50}$ sample as compared to the (110)-oriented one. The larger number of structural defects and grain boundaries of the polycrystalline $Fe_{50}Mn_{50}$ is responsible for the more pronounced decrease of H_{EB} with the cycle number n. The magnitude of the training effect is expected to decrease with increasing temperature.[23]

For the $Ni_{80}Fe_{20}/Fe_{50}Mn_{50}$ bilayers we have used SQUID magnetometry to determine the field cycling number (n) dependence of the vertical shift of the hysteresis loop. As mentioned above, the vertical shift of the hysteresis loop is the consequence of the pinned uncompensated magnetization of the AFM, also referred to as the irreversible DS magnetization.[8] The magnetization of the sole FM layer [a 10 nm thick $Ni_{80}Fe_{20}$ layer grown on a $Si/SiO_2/Cu(50\ nm)$ substrate] was found to be independent of the magnetic field cycling. For each n, the value of the pinned uncompensated magnetization m_{uncomp} of an AFM monolayer is transformed into the fraction f_{uncomp} of the pinned uncompensated moments of a monolayer as follows: $f_{uncomp}=m_{uncomp}/m_{AFM}$, where m_{AFM} is the magnetic moment of a monolayer of the Mn sublattice. For these calculations we have taken into account the different atomic structure of the epitaxial samples, whereas for the polycrystalline sample we have considered the (111) orientation. More details about this estimate are given in Ref. 24. The maximum absolute values of the fraction of AFM (FeMn) pinned uncompensated moments of a monolayer $f_{uncomp}(n=1)$ (measured at $T=5$ K) is about 1.9% for the epitaxial samples and about 2.9% for the polycrystalline sample. These values are in the right order of magnitude as the experimentally determined fraction of pinned interfacial uncompensated monolayer moments of the AFM IrMn (4%) using x-ray magnetic circular dichroism by Ohldag *et al.*[25] and of the AFM CoO (1%) from the SQUID measurements by Takano *et al.*[26]

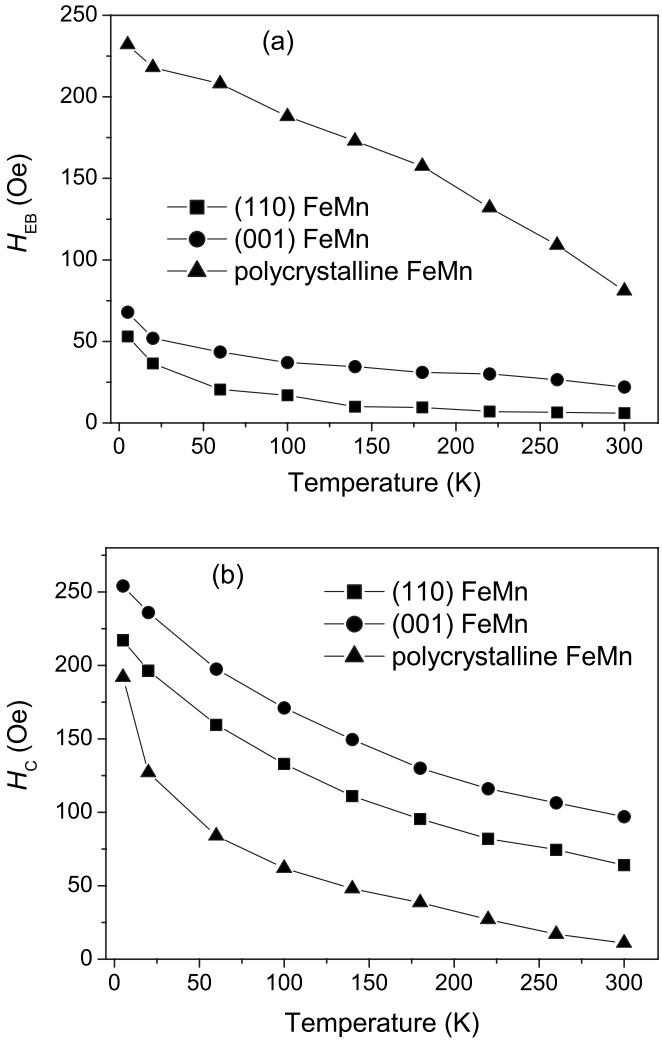

FIG. 4. Temperature dependence of (a) H_{EB} and (b) H_C of the $Ni_{80}Fe_{20}/Fe_{50}Mn_{50}$ bilayers with (110)- and (001)- oriented $Fe_{50}Mn_{50}$, and polycrystalline $Fe_{50}Mn_{50}$ layers.

The value of f_{uncomp} decreases with the number of field cycles n. We illustrate this in Fig. 3(b) where we show the decrease of the fraction of pinned uncompensated moments of an AFM monolayer $f_{uncomp}(n)-f_{uncomp}(n=12)$ as a function of n. We observe that the fraction of pinned uncompensated moments decreases with n in a similar manner as the training effect of H_{EB} [shown in the inset of Fig. 3(b); here we present the non-normalized H_{EB} values from Fig. 2(a)]. We conclude a good correlation between the magnitude of the training effect of H_{EB} [Fig. 2(a) and inset of Fig. 3(b)] and the decrease of the fraction of the pinned uncompensated moments as a function of n [Fig. 3(b)]. These observations strongly suggest that the training effect in the system under consideration is determined by the decrease of the AFM pinned uncompensated magnetization (and consequently of f_{uncomp}). This is in agreement with the DS model.

We have also investigated the temperature dependence of H_{EB} for all three samples and the results are depicted in Fig. 4(a). The data at $T=5$ K in Fig. 4 are those measured for $n=12$. One can observe a monotonic decrease of H_{EB} with increasing temperature for all three samples. For a given

temperature, the polycrystalline sample has the largest values of H_{EB}, up to four times higher in comparison with the epitaxial samples. H_{EB} of the epitaxial samples shows a qualitatively similar temperature dependence with a relatively stronger decrease of H_{EB} at low temperatures followed by a weaker decrease at higher temperatures. At each temperature, the values of H_{EB} of the (001)-oriented sample are slightly higher than the corresponding ones of the (110)-oriented sample. Figure 4(b) shows the temperature dependence of H_C for all three samples. H_C decreases for all samples monotonously with increasing temperature. Moreover, one can see that H_C also depends on the crystalline structure of the bilayers. At each temperature, the highest value of H_C corresponds to the (001)-oriented sample, followed by the one corresponding to the (110)-oriented sample. The smallest value of H_C was observed for the polycrystalline sample, even though this sample shows the highest values of H_{EB} as compared to the epitaxial samples. Hence, the polycrystalline sample is the most attractive one from an application point of view due to the higher H_{EB} and smaller H_C in comparison with the epitaxial samples.

The dependence of H_{EB} on the crystalline structure of the $Fe_{50}Mn_{50}$ layer is interpreted in the framework of the DS model.[8,9] After cooling down the samples in the presence of a magnetic field, a metastable DS is induced in the $Fe_{50}Mn_{50}$ layer. The formation of the DS depends on the degree of structural order in the AFM. Therefore, different kinds of structural and compositional defects[10,22] acting as pinning centers for the AFM domain walls contribute to the creation of the AFM DS. Since the epitaxial growth of (110) $Fe_{50}Mn_{50}$ was observed to be superior compared to the epitaxial growth of (001) $Fe_{50}Mn_{50}$, we expect less defects in the (110) $Fe_{50}Mn_{50}$ as compared to the (001) orientation. This superior quality of the (110) epitaxial $Fe_{50}Mn_{50}$ gives rise to a DS with a reduced number of domain walls. Therefore, the number of uncompensated moments is reduced giving rise to a small H_{EB}. On the other hand, for the polycrystalline $Fe_{50}Mn_{50}$ a structure containing crystalline grains with mean diameter of 18 nm was observed.[10] Under the hypothesis that the grain boundaries act also as domain walls for the AFM domains,[10] it is expected that a larger number of AFM domains as well as a larger number of uncompensated moments are to be found in the polycrystalline $Fe_{50}Mn_{50}$. This gives rise to the larger H_{EB} values of the polycrystalline sample in comparison with the ones of the epitaxial samples. On the other hand, the smaller crystalline grains of the polycrystalline sample as compared to the epitaxial samples also have an important impact on the coercivity of the bilayers. According to the random anisotropy model,[7,27] the smaller the FM grain size, the lower is the FM coercivity. This explains why the coercivity of the polycrystalline sample is lower than that of the epitaxial samples [Fig. 4(b)]. The different values of H_C of the two epitaxial samples could also be a consequence of different grain sizes of the two epitaxial samples. However, the determination of such grain sizes is beyond the scope of our techniques.

IV. CONCLUSIONS

In conclusion, we have shown that both H_{EB} and H_C of $Ni_{80}Fe_{20}/Fe_{50}Mn_{50}$ bilayers grown on different substrates show a magnetic training effect. The magnitude of the training effect depends on the crystalline structure of $Fe_{50}Mn_{50}$. It is larger for the polycrystalline sample and decreases in magnitude with increasing quality of the epitaxial growth. The training effect was found to originate from the cycle-number dependence of H_1, the switching field of the descending branch of the hysteresis loop. A very good qualitative agreement between the decrease of the fraction of pinned uncompensated moments of an AFM monolayer and the decrease of H_{EB} as a function of the hysteresis cycle number (n) was found. H_{EB} and H_C of all three samples decrease with increasing temperature, but at each temperature H_{EB} of the polycrystalline sample is larger as compared to H_{EB} of the epitaxial samples. On the other hand, at each temperature the coercive field of the polycrystalline sample shows the smallest values as compared to the epitaxial samples. The results can be explained in the framework of the DS model taking into account the quality of the crystal growth and the grain structure of the $Ni_{80}Fe_{20}/Fe_{50}Mn_{50}$ bilayers.

ACKNOWLEDGMENTS

The authors would like to thank K. O'Grady and C. Smits for critical reading of the manuscript and for their comments. The financial support received in the framework of the EU NEXBIAS Research Training Network (Contract No. HPRN-CT-2002-00296) is gratefully acknowledged.

[1] W. H. Meiklejohn and C. P. Bean, Phys. Rev. **105**, 904 (1957).
[2] J. Nogues and I. K. Schuller, J. Magn. Magn. Mater. **192**, 203 (1999).
[3] A. E. Berkowitz and K. Takano, J. Magn. Magn. Mater. **200**, 552 (1999).
[4] M. Kiwi, J. Magn. Magn. Mater. **234**, 584 (2001).
[5] E. Fulcomer and S. H. Charap, J. Appl. Phys. **43**, 4184 (1972).
[6] D. Mauri, H. C. Siegmann, P. S. Bagus, and E. Kay, J. Appl. Phys. **62**, 3047 (1987).
[7] A. P. Malozemoff, Phys. Rev. B **35**, 3679 (1987).
[8] U. Nowak, K. D. Usadel, J. Keller, P. Miltenyi, B. Beschoten, and G. Güntherodt, Phys. Rev. B **66**, 014430 (2002).
[9] J. Keller, P. Miltenyi, B. Beschoten, G. Güntherodt, U. Nowak, and K. D. Usadel, Phys. Rev. B **66**, 014431 (2002).
[10] C. Papusoi, J. Hauch, M. Fecioru-Morariu, and G. Güntherodt, J. Appl. Phys. **99**, 123902 (2006).
[11] M. Fecioru-Morariu, S. R. Ali, C. Papusoi, M. Sperlich, and G. Güntherodt, Phys. Rev. Lett. **99**, 097206 (2007).
[12] T. C. Schulthess, W. H. Butler, G. M. Stocks, S. Maat, and G. J. Mankey, J. Appl. Phys. **85**, 4842 (1999).
[13] G. M. Stocks, W. A. Shelton, T. C. Schulthess, B. Ujfalussy, W. H. Butler, and A. Canning, J. Appl. Phys. **91**, 7355 (2002).

[14] R. Jungblut, R. Coehoorn, M. T. Johnson, J. aan de Stegge, and A. Reinders, J. Appl. Phys. **75**, 6659 (1994).
[15] R. Jungblut, R. Coehoorn, M. T. Johnson, Ch. Sauer, P. J. van der Zaag, A. R. Ball, Th. G. S. M. Rijks, J. aan de Stegge, and A. Reinders, J. Magn. Magn. Mater. **148**, 300 (1995).
[16] A. Hoffmann, Phys. Rev. Lett. **93**, 097203 (2004).
[17] M. Ali, C. H. Marrows, and B. J. Hickey, Phys. Rev. B **67**, 172405 (2003).
[18] H. Xi, R. M. White, S. Mao, Z. Gao, Z. Yang, and E. Murdock, Phys. Rev. B **64**, 184416 (2001).
[19] T. Hauet, J. A. Borchers, Ph. Mangin, Y. Henry, and S. Mangin, Phys. Rev. Lett. **96**, 067207 (2006).
[20] A. Hochstrat, Ch. Binek, and W. Kleemann, Phys. Rev. B **66**, 092409 (2002).
[21] F. Radu, M. Etzkorn, T. Schmitte, R. Siebrecht, A. Schreyer, K. Westerholt, and H. Zabel, J. Magn. Magn. Mater. **240**, 251 (2002).
[22] M. R. Ghadimi, B. Beschoten, and G. Güntherodt, Appl. Phys. Lett. **87**, 261903 (2005).
[23] B. Beschoten, J. Keller, A. Tillmanns, and G. Güntherodt, IEEE Trans. Magn. **38**, 2744 (2002).
[24] The pinned uncompensated moment of an AFM monolayer is calculated as $m_{\mathrm{uncomp}}=m_{\mathrm{SQUID}}/(t_{\mathrm{AFM}}/d_p)$, where m_{SQUID} is the total pinned uncompensated AFM magnetization measured by SQUID, t_{AFM} is the thickness of the AFM layer, and d_p is the perpendicular lattice spacing of the AFM. The values of d_p for γ-$Fe_{50}Mn_{50}$ with different orientations were taken from Ref. 14. In order to calculate m_{AFM} we considered a sublattice of Mn atoms and calculated its magnetic moment as being $3.4\mu_{\mathrm{B}}\cdot 0.5\cdot N$, where N depends on the crystalline orientation of the AFM and represents the total number of atoms of an AFM monolayer.
[25] H. Ohldag, A. Scholl, F. Nolting, E. Arenholz, S. Maat, A. T. Young, M. Carey, and J. Stöhr, Phys. Rev. Lett. **91**, 017203 (2003).
[26] K. Takano, R. H. Kodama, A. E. Berkowitz, W. Cao, and G. Thomas, Phys. Rev. Lett. **79**, 1130 (1997).
[27] G. Herzer, IEEE Trans. Magn. **26**, 1397 (1990).